J. Fluid Mech. (2016), *vol.* 805, R4, doi:10.1017/jfm.2016.578

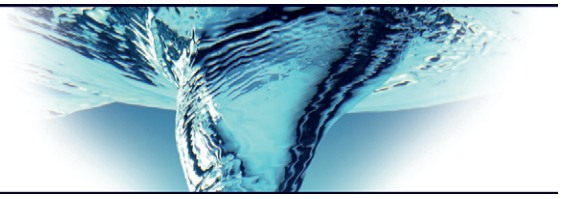

JFM RAPIDS
journals.cambridge.org/rapids

Exploring the severely confined regime in Rayleigh–Bénard convection

Kai Leong Chong[1] **and Ke-Qing Xia**[1,†]

[1]Department of Physics, The Chinese University of Hong Kong, Shatin, Hong Kong, China

(Received 11 July 2016; revised 19 August 2016; accepted 26 August 2016;
first published online 23 September 2016)

We study the effect of severe geometrical confinement in Rayleigh–Bénard convection with a wide range of width-to-height aspect ratio Γ, $1/128 \leqslant \Gamma \leqslant 1$, and Rayleigh number Ra, $3 \times 10^4 \leqslant Ra \leqslant 1 \times 10^{11}$, at a fixed Prandtl number of $Pr = 4.38$ by means of direct numerical simulations in Cartesian geometry with no-slip walls. For convection under geometrical confinement (decreasing Γ from 1), three regimes can be recognized (Chong *et al.*, *Phys. Rev. Lett.*, vol. 115, 2015, 264503) based on the global and local properties in terms of heat transport, plume morphology and flow structures. These are Regime I: classical boundary-layer-controlled regime; Regime II: plume-controlled regime; and Regime III: severely confined regime. The study reveals that the transition into Regime III leads to totally different heat and momentum transport scalings and flow topology from the classical regime. The convective heat transfer scaling, in terms of the Nusselt number Nu, exhibits the scaling $Nu - 1 \sim Ra^{0.61}$ over three decades of Ra at $\Gamma = 1/128$, which contrasts sharply with the classical scaling $Nu - 1 \sim Ra^{0.31}$ found at $\Gamma = 1$. The flow in Regime III is found to be dominated by finger-like, long-lived plume columns, again in sharp contrast with the mushroom-like, fragmented thermal plumes typically observed in the classical regime. Moreover, we identify a Rayleigh number for regime transition, $Ra^* = (29.37/\Gamma)^{3.23}$, such that the scaling transition in Nu and Re can be clearly demonstrated when plotted against Ra/Ra^*.

Key words: Bénard convection, Hele-Shaw flows, low-Reynolds-number flows

1. Introduction

Rayleigh–Bénard (RB) convection occurs in a fluid layer heated from below and cooled from above when the temperature difference is sufficient to initiate instability. This classical paradigm has far-reaching implications for industrial processes, and for fundamental physics in astrophysical and geophysical convections, and its importance

† Email address for correspondence: kxia@cuhk.edu.hk

is testified to by the large number of studies over the past decade (Ahlers, Grossmann & Lohse 2009; Lohse & Xia 2010; Chillà & Schumacher 2012; Xia 2013). Convective heat transfer, in terms of the Nusselt number Nu, is a fundamental issue in thermal convection, and it has been widely accepted that the heat exchange in RB convection is dictated by the thermal plumes. Typically, plumes organize themselves into the so-called large-scale circulation (LSC) to efficiently transport heat across the convection cell (Kadanoff 2001; Shang *et al.* 2003; Xi, Lam & Xia 2004), and this mechanism is regarded as the standard mode of heat transfer in classical RB convection for a closed convection cell of aspect ratio around one.

The geometric properties, such as the cell geometry and the lateral extent (characterized by the aspect ratio Γ), strongly influence the LSC and thus the motion of plumes. An example for the influence of cell geometry is that in a cylindrical cell of aspect ratio around one the LSC is manifested as a single-roll structure meandering azimuthally (Cioni, Ciliberto & Sommeria 1997; Brown, Nikolaenko & Ahlers 2005; Sun, Xi & Xia 2005*b*; Xi, Zhou & Xia 2006), but it becomes largely confined along the cell diagonal when cubic cells are used instead. Besides the shape of cell, varying Γ is the alternative method for changing the nature of LSC. As Γ is increased from one, the original single-roll structure becomes multi-roll (Funfschilling *et al.* 2005; Sun *et al.* 2005*a*). As Γ is decreased from one, LSC will be strongly suppressed by the closer no-slip walls, as reflected by more frequent flow reversals in quasi-2D convection (Ni, Huang & Xia 2015; Huang & Xia 2016). One question is whether the distinct flow patterns brought about by changing geometric parameters would also influence the convective heat transfer, through a possible modification of plume properties. This leads to the study of geometrical effect on heat transport in RB convection (Grossmann & Lohse 2003; Ching & Tam 2006; Bailon-Cuba, Emran & Schumacher 2010; van der Poel *et al.* 2012; Zhou *et al.* 2012; Huang *et al.* 2013; Wagner & Shishkina 2013; Chong *et al.* 2015). A number of experimental studies in fluids with $Pr > 1$ (e.g. water) have found that heat transport in RB convection is actually insensitive to the nature of LSC (Wu & Libchaber 1992; Xia & Lui 1997; Funfschilling *et al.* 2005; Nikolaenko *et al.* 2005; Zhou *et al.* 2012). These observations can be understood as follows. The thermal boundary layer is buffered by a thicker viscous boundary layer in the case of $Pr > 1$ (van der Poel, Stevens & Lohse 2011). However, by reducing Γ to much less than one, Huang *et al.* (2013) and Chong *et al.* (2015) have discovered something highly non-trivial – heat flux increases significantly under geometrical confinement. Chong *et al.* (2015) have furthermore found three regimes based on the various heat transport behaviours: Regime I: classical boundary-layer-controlled regime in which heat flux is insensitive to the change in Γ; Regime II: plume-controlled regime in which heat flux increases significantly with decreasing Γ owing to the increased plume coherency; and Regime III: severely confined regime in which heat flux drops dramatically with decreasing Γ. The present study further shows that Regime III should be restricted to cases well above the onset of convection in which Nu–Ra possesses steep scaling. We remark that the three regimes were previously recognized for $Pr = 4.38$, but the regime transition may depend on Pr as well. For $Pr = 0.786$, the 3D simulations with $10^5 \leqslant Ra \leqslant 10^9$ by Wagner & Shishkina (2013) have shown that decreasing Γ can lead to a significant drop in Nu, but Regime II has not been realized for their explored parameter range.

Previous studies of highly confined RB convection ($\Gamma \ll 1$) have mainly considered how Nu responds to a reducing Γ, while ignoring the question of whether heat transport scaling of Nu versus Rayleigh number Ra would differ in the three regimes.

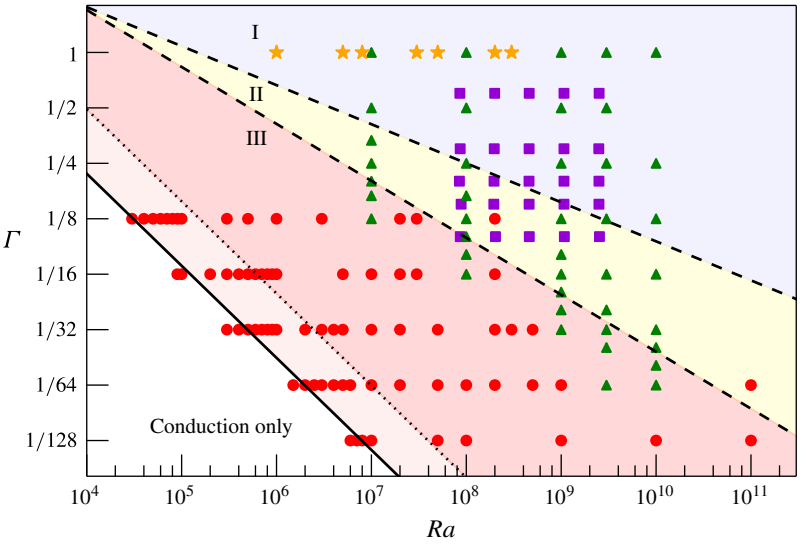

FIGURE 1. Phase diagram of different regimes of heat transport under geometrical confinement. I represents the classical boundary-layer-controlled regime; II represents the plume-controlled regime; and III represents the severely confined regime. The dashed line separating I and II is $\Gamma = 12.42Ra^{-0.21}$, which is determined by the spacing between plumes, and that separating II and III is $\Gamma = 29.37Ra^{-0.31}$, which is identified by the optimal aspect ratio for achieving the maximum Nu (Chong *et al.* 2015). The solid line is $Ra = Ra_c$, with $Ra_c = 482.4\Gamma^{-2.0\pm0.1}$, which indicates the onset Ra for different Γ; and the dotted line is $Ra = 5Ra_c$. Note that $Ra_c \leqslant Ra \leqslant 5Ra_c$ is the transition region before reaching Regime III. Purple squares and green triangles denote the experimental and DNS data from Huang *et al.* (2013) and Chong *et al.* (2015), respectively. Orange stars denote the DNS data for cubic geometry from Kaczorowski & Xia (2013) as a baseline for comparing with the confined cases. Red circles represent the new simulations performed in the present study. All cases are for fluid with $Pr = 4.38$.

One of the few experimental studies on highly confined RB convection (Huang & Xia 2016) has provided a Nu–Ra relationship in Regime II, in which the classical scaling with exponents between $1/4$ and $1/3$ is found. Those authors analysed the bulk and boundary layer contributions to the scaling in terms of the model of Grossmann & Lohse (2000, 2001) and found that the weight of the boundary layer contribution relative to the bulk contribution increases with decreasing Γ. However, Regime III has been barely touched in previous studies (see figure 1), so the Nu–Ra relation in this regime remains unexplored.

In the present study we have conducted highly resolved direct numerical simulations (DNS) of confined Rayleigh–Bénard convection over a large region of the parameter space, with the aspect ratio spanning over two decades and the Rayleigh number spanning seven decades. The width-to-height aspect ratio Γ has been reduced to as low as $1/128$ to fully explore the severely confined regime (Regime III). With such small Γ, Regime III could be explored for almost four decades of Ra, which enabled us to investigate the scalings of Nu and the Reynolds number Re with Ra in Regime III and the corresponding flow topologies.

2. Numerical procedure and set-ups

The simulation determines the non-dimensional velocities $\boldsymbol{u} = (u_x, u_y, u_z)$ with the temperature field T for the incompressible flow by numerically integrating the three-dimensional Navier–Stokes equations in Cartesian geometry within the Oberbeck–Boussinesq approximation,

$$\partial \boldsymbol{u}/\partial t + \boldsymbol{u}\cdot\boldsymbol{\nabla}\boldsymbol{u} + \boldsymbol{\nabla} p = (Pr/Ra)^{1/2}\nabla^2\boldsymbol{u} + T\boldsymbol{z}, \tag{2.1}$$

$$\partial T/\partial t + \boldsymbol{u}\cdot\boldsymbol{\nabla} T = (PrRa)^{-1/2}\nabla^2 T, \tag{2.2}$$

$$\boldsymbol{\nabla}\cdot\boldsymbol{u} = 0, \tag{2.3}$$

where $Ra = \alpha g \Delta T H^3/\nu\kappa$ and $Pr = \nu/\kappa$ are the Rayleigh number and the Prandtl number with α, ν and κ denoting the thermal expansion coefficient, kinematic viscosity and thermal diffusivity of fluid; g is the gravitational acceleration and ΔT the temperature difference across the system height H. The equations are solved in non-dimensional form by using the system height H, free-fall velocity $\sqrt{\beta g \Delta T H}$ and global temperature difference ΔT as the respective normalization scales. In this dimensionless form, the range of temperature should be $-0.5 \leqslant T \leqslant 0.5$. The velocity boundary conditions of the simulations are that all walls are no-slip and impermeable. And the temperature boundary conditions are that the sidewall is adiabatic while the top and bottom surfaces are isothermal with top (bottom) surface fixed at $T = -0.5$ ($T = 0.5$).

The code solves the equations through the finite-volume method on a staggered grid with fourth-order accuracy in space. The convective and diffusive terms in the equations are temporally advanced by the leapfrog and Euler forward methods respectively. A major concern for DNS in RB convection is to resolve the smallest relevant scale in turbulent flows, which is either the Kolmogorov length η_k or the Batchelor length η_b depending on whether $Pr < 1$ or $Pr > 1$. The global estimations of both length scales in dimensionless form are expressed as $\eta_k = \sqrt{Pr}/[Ra(Nu-1)]^{1/4}$ and $\eta_b = 1/[Ra(Nu-1)]^{1/4}$, and this implies that the number of grid points necessary along a dimension roughly doubles when Ra increases tenfold. Due to the non-uniform distribution of the length scales over space, a stricter resolution requirement is needed near the boundary layers (Shishkina *et al.* 2010). Those requirements were taken into consideration to perform reliable simulations, and therefore $N_z = 2304$ grid points have been adopted along the vertical direction for our largest explored Ra ($= 1 \times 10^{11}$). The results were collected when the simulations had reached the statistical steady state as judged by the convergence of global Nu over time. For details of the code validation, details of the numerical scheme and an *a priori* check on the grid design, we refer to the previous publications (Kaczorowski *et al.* 2008; Kaczorowski & Xia 2013; Kaczorowski, Chong & Xia 2014).

We present the result from 100 cases in total, 74 cases from the new simulations combined with 26 cases from our previous numerical data sets (Kaczorowski & Xia 2013; Chong *et al.* 2015), with the width-to-height aspect ratio Γ spanning over two decades ($1/128 \leqslant \Gamma \leqslant 1$) while the length-to-height aspect ratio is kept fixed at 1, Ra spans almost seven decades ($3 \times 10^4 \leqslant Ra \leqslant 1 \times 10^{11}$) and Pr is fixed at $Pr = 4.38$. To focus on the severely confined regime, five small Γ values are studied in detail here ($\Gamma = 1/8$, $1/16$, $1/32$, $1/64$ and $1/128$), together with $\Gamma = 1$ cases as the baseline. The Ra–Γ combination of the new simulations and our previous data sets are summarized in the phase diagram shown in figure 1.

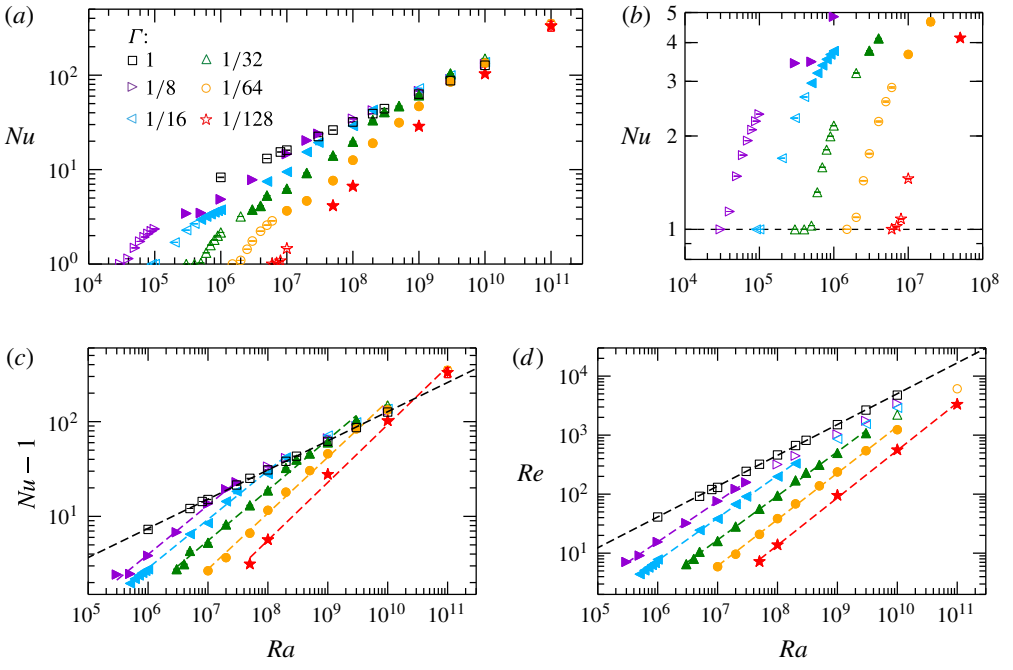

FIGURE 2. (*a*,*b*) Nu versus Ra, (*c*) $Nu-1$ versus Ra and (*d*) Re versus Ra for $\Gamma=1$, 1/8, 1/16, 1/32, 1/64 and 1/128. The dashed lines are power-law fittings under the scheme: the data within $5Ra_c \leqslant Ra \leqslant Ra^*$ are fitted for $\Gamma \leqslant 1/8$ (represented as solid symbols) where Ra_c is the onset Ra and Ra^* is the Ra for transition between Regimes II and III, while the full range of Ra is used for $\Gamma=1$. Note that to focus on the scaling observed well above the onset, data with $Ra < 5Ra_c$ are not shown in (*c*,*d*).

3. Results and discussion

The first important quantity to be examined is the global convective heat flux, expressed as $Nu-1$ where $Nu-1=0$ represents the case of pure conduction. The heat flux across a horizontal plane can be calculated through $Nu_s = \langle (RaPr)^{1/2} u_z T - \partial T/\partial z \rangle_{x,y,t}$, where $\langle . \rangle_{x,y,t}$ represents the averaging over the horizontal plane and a sufficiently long period of time. Nu is estimated by averaging Nu_s over every horizontal plane. Besides the direct measurement of heat flux, Nu can also be estimated from the exact relations with the globally averaged viscous and thermal dissipation rates, which are $Nu = \langle \epsilon_u \rangle (RaPr)^{1/2} + 1$ and $Nu = \langle \epsilon_T \rangle (RaPr)^{1/2}$, with $\langle . \rangle$ representing averaging over the entire domain and infinite time, $\epsilon_u = (Ra/Pr)^{-1/2} \sum_i \sum_j (1/2)(\partial u_i/\partial x_j + \partial u_j/\partial x_i)^2$ and $\epsilon_T = (RaPr)^{-1/2} \sum_i (\partial T/\partial x_i)^2$. Here the average of the three values is taken as the numerically measured Nu and their standard deviation represents the error. Another important global transport quantity is the Reynolds number Re, which characterizes the flow intensity and is defined as $\sqrt{\langle \boldsymbol{u}^2 \rangle}(Ra/Pr)^{1/2}$ (note that the large-scale flow velocity is ill-defined for small Γ because the LSC has been strongly suppressed for highly confined cases).

In order to capture the onset Rayleigh number Ra_c for convection, we first examine Nu versus Ra in figure 2(*a*,*b*) instead of $Nu-1$ versus Ra. The Ra_c for each case of small Γ between 1/128 and 1/8 is identified based on the fact that Nu settles at one when Ra is below Ra_c, and the values are listed in table 1. We find that Ra_c obeys a

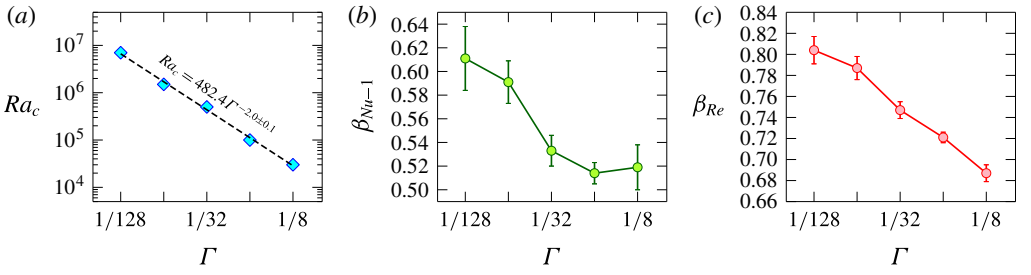

FIGURE 3. (*a*) Onset Rayleigh number Ra_c versus Γ. Exponents for the power laws $Nu - 1 \sim Ra^{\beta_{Nu-1}}$ and $Re \sim Ra^{\beta_{Re}}$ in the severely confined regime versus Γ: (*b*) β_{Nu-1} and (*c*) β_{Re}, with the lines drawn to guide the eye.

Γ	Ra_c	β_{Nu-1}	β_{Re}
1/8	3×10^4	0.52 ± 0.02	0.69 ± 0.01
1/16	1×10^5	0.51 ± 0.01	0.72 ± 0.00
1/32	5×10^5	0.53 ± 0.01	0.75 ± 0.01
1/64	1.5×10^6	0.59 ± 0.02	0.79 ± 0.01
1/128	7×10^6	0.61 ± 0.03	0.80 ± 0.01

TABLE 1. Onset Rayleigh number Ra_c and scaling exponents from the relations $Nu - 1 \sim Ra^{\beta_{Nu-1}}$ and $Re \sim Ra^{\beta_{Re}}$ fitted to data lying in the severely confined regime.

power-law relation with Γ, i.e. $Ra_c = 482.4\Gamma^{-2.0\pm0.1}$ (figure 3*a*). This scaling exponent agrees excellently with $Ra_c \sim \Gamma^{-2}$ (for $\Gamma \ll 1$), which was derived from linear stability analysis that was originally developed for Hele-Shaw convection (Bizon *et al.* 1997). Figure 2(*a*,*b*) also reveals that, after Ra exceeds Ra_c, there exists a transition region for Nu before it clearly exhibits a power-law behaviour. In this work, we mainly focus on the scaling relation that occurs for Ra well above Ra_c. Thus, only the data points with $Ra \geqslant 5Ra_c$ are included for scaling analysis.

Figure 2(*c*) plots $Nu - 1$ versus Ra for different Γ on a log–log scale, which readily shows the power-law relation. As a baseline we first examine the case for $\Gamma = 1$ (black squares). The power-law fitting represented by the black dashed line yields $Nu - 1 = 0.106Ra^{0.308\pm0.001}$ over the full range of explored Ra, $1 \times 10^6 \leqslant Ra \leqslant 1 \times 10^{10}$, indicating that the scaling in this range for the case of $\Gamma = 1$ can be described by a single power law. For the confined cases ($\Gamma \leqslant 1/8$) and over the range of Ra explored, the convective state may straddle various regimes in the phase diagram shown in figure 1, implying the possibility of having multiple scalings. Indeed, as can be clearly seen from figure 2(*c*), data for the cases of small Γ exhibit different scaling behaviours as Ra increases. The sharp change of scaling takes place at the boundary separating Regime II and Regime III, i.e. $\Gamma = 29.37Ra^{-0.31}$ (Chong *et al.* 2015), which leads us to identify a Rayleigh number for this regime transition, $Ra^* = (29.37/\Gamma)^{3.23}$. We fit the data for individual Γ separately for data points with $Ra < Ra^*$ (represented by the solid symbols), with the fitting indicated by the dashed lines in corresponding colours in figure 2(*c*,*d*). For instance, the case of $\Gamma = 1/128$ (red star) exhibits the scaling exponent of 0.61 over three decades of Ra ($5 \times 10^7 \leqslant Ra \leqslant 1 \times 10^{11}$), which is much larger than 0.31 for $\Gamma = 1$. We also examine Re similarly (figure 2*d*), which yields the scaling $Re \sim Ra^{0.80\pm0.01}$ for

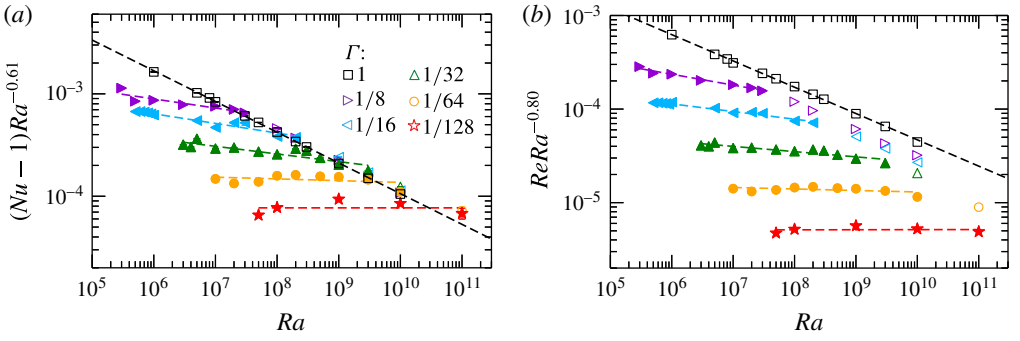

FIGURE 4. Compensated plots of (*a*) $(Nu-1)Ra^{-0.61}$ and (*b*) $ReRa^{-0.80}$ versus Ra for six values of Γ between 1/128 and 1. The power-law fitting is the same as in figure 2.

$\Gamma = 1/128$, contrasting sharply with the scaling $Re \sim Ra^{0.522\pm0.003}$ for $\Gamma = 1$. Details of the fitting exponents in the severely confined regime (Regime III) for each Γ are shown in table 1 and plotted in figure 3(*b*,*c*). It is seen that the scaling exponents for both Nu and Re increase with decreasing Γ in Regime III. The exponents also seem to approach some asymptotic values, and for the sake of discussion we take the exponents for $\Gamma = 1/128$ (smallest value explored) as the proxy for those values. To verify this, it will be highly desirable to have 3D simulations for Γ much smaller than 1/128 in the future. However, it will be a difficult task for DNS because of the infinitesimally small time step needed for small grid spacing along the confinement direction for $\Gamma \ll 1$.

The above scaling behaviour can be shown more clearly by the compensated plots. Figure 4(*a*) displays $(Nu-1)Ra^{-0.61}$ versus Ra, which also demonstrates that the scaling in the severely confined regime is not strictly universal (before entering the asymptotic state). Figure 4(*a*) also clearly demonstrates that, on increasing Ra, the steep scaling observed in Regime III returns to the classical scaling (black dashed line) upon entering the plume-controlled regime (Regime II), which is more evident for the cases $\Gamma = 1/8$ and $\Gamma = 1/16$. The return to the classical scaling in Regime II is actually in agreement with the previous experimental finding (Huang & Xia 2016). Similarly, the compensated plot of $ReRa^{-0.80}$ versus Ra (figure 4*b*) also reveals how the scaling tends from 0.69 to 0.80 as Γ decreases from 1/8 to 1/128, and how the steep scaling in the severely confined regime transits to the classical scaling (black dashed line).

The scaling transition observed for the global quantities may be associated with changes in flow topology. Figure 5 shows slices of the instantaneous dimensionless temperature field taken at the vertical mid-plane, where the reddish and bluish colours represent hot and cold plumes respectively. Figure 5(*a*,*b*,*c*) shows the temperature fields for $\Gamma = 1$ at $Ra = 1 \times 10^8$, 1×10^9 and 1×10^{10} respectively, which are examples of the flow topology in the classical 'less confined' situation. The figures clearly demonstrate that thermal plumes of mushroom-like morphology detach from the top and bottom thermal boundary layers. These plumes cluster mainly on either side of the wall as they are driven by the LSC (note that the main circulating plane of LSC is along the diagonal). With Ra increasing from 1×10^8 to 1×10^{10}, figure 5(*c*) demonstrates that plumes become more fragmented (Zhou & Xia 2010), suggesting smaller scales being excited by stronger thermal forcing. For $\Gamma = 1/32$, as shown in figure 5(*d*–*f*), plumes extending the entire cell height have been observed

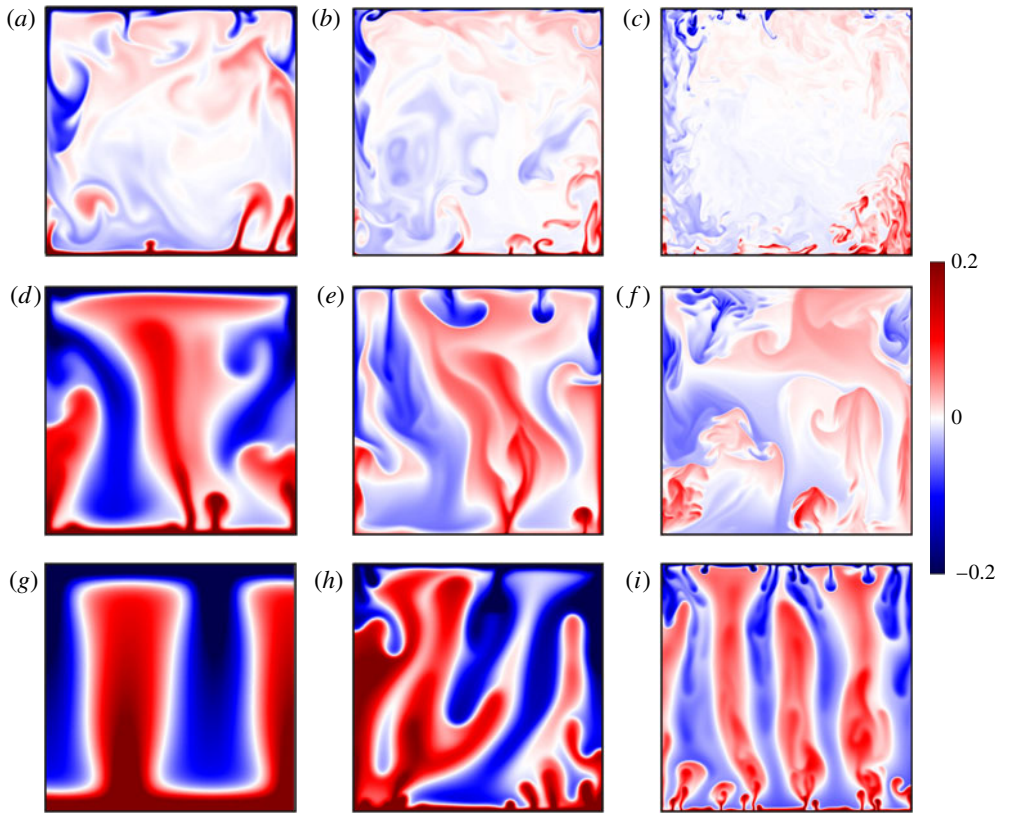

FIGURE 5. Colour-graded instantaneous field of the dimensionless temperature T taken at vertical mid-plane (midway along the confinement direction) for three different Ra, 1×10^8 (a,d,g), 1×10^9 (b,e,h) and 1×10^{10} (c,f,i), and for three different Γ, $\Gamma = 1$ (a–c), $\Gamma = 1/32$ (d–f) and $\Gamma = 1/128$ (g–i). Here the reddish colour indicates the hot fluid while the bluish colour indicates the cold fluid.

for $Ra = 1 \times 10^8$ and 1×10^9, which are cases in the severely confined regime; whereas highly coherent plumes have been observed for $Ra = 1 \times 10^{10}$, in which convective flow has entered the plume-controlled Regime II. The flow topology in severely confined Regime III has also been demonstrated by the smallest explored Γ ($= 1/128$) as shown in figure 5(g–i). It can be seen that the main feature of flow topology becomes the finger-like columns of hot and cold thermal plumes, in contrast to the typical picture of mushroom-like fragmented thermal plumes in the classical regime. Thus, the transition into Regime III leads to the formation of the long-lived columns of thermal plumes that extend the entire cell height. With increasing Ra, not only does the scale of the heat columns become smaller, the columns also become less straight, which is the signature of vanishing vertical coherency as the flow becomes more unstable under stronger thermal driving. Furthermore, figure 5(i) demonstrates a state where mushroom-like plumes grow into column-like plumes; this coalescence of plumes has also been found in a porous medium (Hewitt, Neufeld & Lister 2012). At even larger Ra, the plume-controlled regime should be reached and the dominating feature becomes the highly coherent giant plumes (Huang *et al.* 2013; Chong *et al.* 2015), and eventually the fragmented plumes.

Our study has revealed a new state of thermal convection in which the scaling of the global quantities and the flow topology are strikingly different from their classical counterparts. With sufficiently small Γ and a sufficiently wide range in Ra, thus giving rise to a sufficiently wide Regime III, the transition from Regime III to Regime II and Regime I can be clearly observed from the scalings of the global heat and momentum transport. Also, Regime III possesses a new type of flow topology in the form of column-like plumes. The emergence of finger-like, long-lived heat columns observed here and the multiple transitions in highly confined RB convection observed by Chong *et al.* (2015) are a result of the interplay between stabilizing and destabilizing forces, i.e. the viscous drag from walls as a result of severe confinement and the thermal driving force. It is interesting to note that similarities exist between the present system and other types of convective flows under different forms of stabilizing and destabilizing forces, such as rotating RB convection (Stevens *et al.* 2009; King, Stellmach & Aurnou 2012; Wei, Weiss & Ahlers 2015) and double diffusive convection (Yang, Verzicco & Lohse 2016), in which the forces that suppress the convective flow are the rotation and the stabilizing scalar gradient respectively. For rotating RB convection under vigorous rotation, there exists a regime with convective Taylor columns (Grooms *et al.* 2010), and such columnar flow topology is associated with a very steep Nu–Ra scaling, having an exponent as large as 3.6 when the Ekman number Ek reaches 10^{-7} (Cheng *et al.* 2015). Such a scaling transition in rotating RB convection is related to the crossing of Ekman and thermal boundary layers, and a rescaled Rayleigh number $Ra\,Ek^{3/2}$ has been introduced (King *et al.* 2012) to understand the observed Nu behaviour. Here, for severely confined RB convection, the new scaling is found in Regime III, which is entered when Ra is smaller than a Γ-dependent value $Ra^* = (29.37/\Gamma)^{3.23}$. Therefore, a rescaled Rayleigh number $Ra/Ra^* = 1.84 \times 10^{-5} Ra\Gamma^{3.23}$ may be suitable for revealing the regime transition.

With the rescaled Ra, the compensated plot $(Nu - 1)Ra^{-0.31}$ collapsed onto more or less a single curve whereas the plot $(Nu - 1)Ra^{-0.61}$ can also be collapsed by multiplying by a Γ-dependent shift factor C_1, where its Γ-dependence is shown in figure 6(*a*). Similar to Nu, the plots of $Re\,Ra^{-0.52}$ and $Re\,Ra^{-0.80}$ use the shift factors C_2 and C_3 for collapsing the data, and the Γ-dependence of these factors is shown in figure 6(*b*,*c*). Interestingly, C_1, C_2 and C_3 all have a power-law dependence on Γ, with the coefficients all close to one, i.e. $C_1 = 1.06\Gamma^{-0.88\pm0.02}$, $C_2 = 0.88\Gamma^{-0.31\pm0.03}$ and $C_3 = 0.86\Gamma^{-1.23\pm0.04}$. After determining the power-law dependence on Γ, the compensated $(Nu - 1)Ra^{-0.31}$ and $(Nu - 1)Ra^{-0.61}\Gamma^{-0.88}$, using exponents for the classical and severely confined regimes, are plotted versus the rescaled Rayleigh number Ra/Ra^* in figure 6(*d*,*e*). The results clearly demonstrate the crossover of the Nu scaling. For $Ra > Ra^*$ over the explored range of Ra, the curves follow the classical scaling. And for $Ra < Ra^*$, the scaling becomes much steeper than the classical one. Figure 6(*e*) shows the compensated plot by using the exponent 0.61 corresponding to the smallest explored Γ ($\Gamma = 1/128$), and thus the curve for $\Gamma = 1/128$ is flat for $Ra < Ra^*$, whereas curves for $\Gamma > 1/128$ are not totally flat for $Ra < Ra^*$ but sufficient to indicate the steep scaling in severely confined regimes in contrast to the classical scaling. Similar behaviours are observed for the global momentum transport Re. Figure 6(*f*,*g*) shows the compensated $Re\,Ra^{-0.52}\Gamma^{-0.31}$ and $Re\,Ra^{-0.80}\Gamma^{-1.23}$, again using exponents for the classical and severely confined regimes respectively, versus the rescaled Ra, which demonstrates the clear transition at $Ra = Ra^*$. We note that the collapsing of the data for Re is less good than that for Nu; this may be related to the fact that the definition of the Reynolds number is scale-dependent and confinement may have changed the characteristic scale for the Reynolds number.

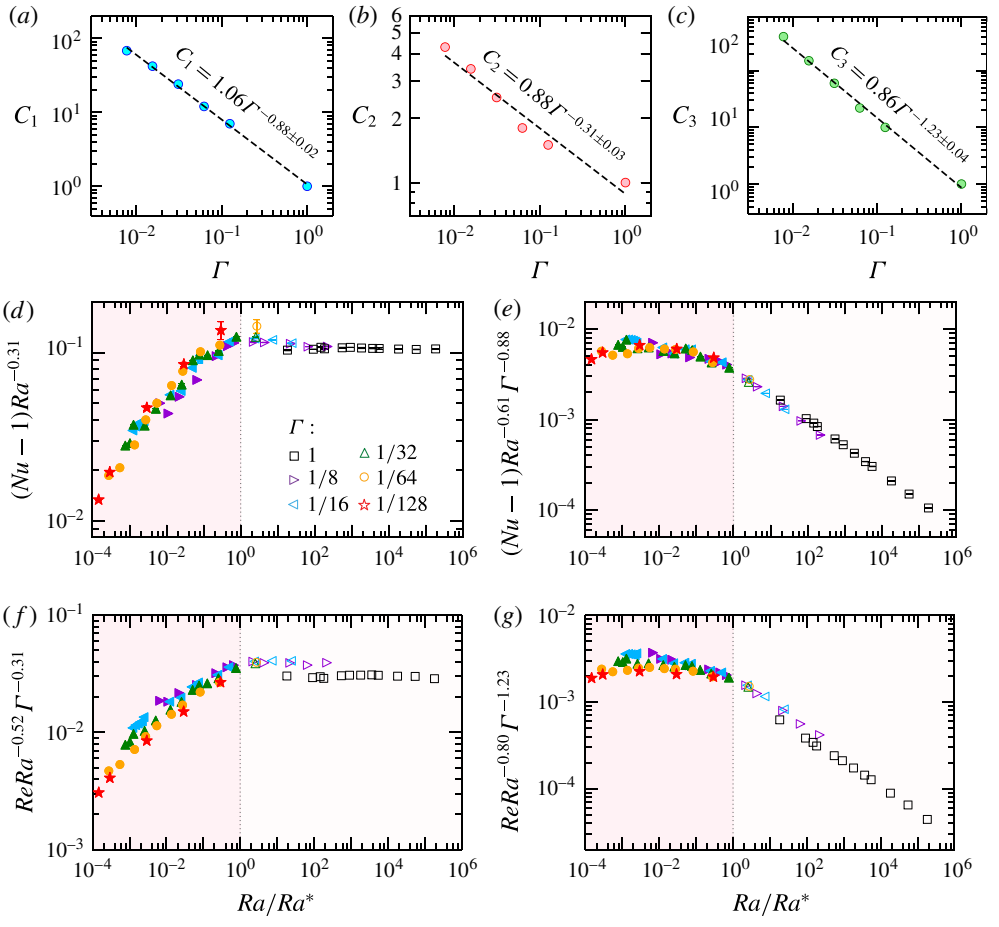

FIGURE 6. The shift factors C_1, C_2 and C_3 versus Γ in (*a*), (*b*) and (*c*), respectively. Here C_1, C_2 and C_3 are arbitrarily chosen factors such that $C_1(\Gamma)(Nu-1)Ra^{-0.61}$, $C_2(\Gamma)Re\,Ra^{-0.52}$ and $C_3(\Gamma)Re\,Ra^{-0.80}$ collapse onto more or less single curves. Compensated plots of (*d*) $(Nu-1)Ra^{-0.31}$, (*e*) $(Nu-1)Ra^{-0.61}\Gamma^{-0.88}$, (*f*) $Re\,Ra^{-0.52}\Gamma^{-0.31}$ and (*g*) $Re\,Ra^{-0.80}\Gamma^{-1.23}$ versus the rescaled Rayleigh number $Ra/Ra^* = 1.84\times10^{-5}Ra\Gamma^{3.23}$ for six different values of Γ. Here the grey dotted line indicates the boundary separating Regimes III and II as found by Chong *et al.* (2015).

4. Concluding remarks

In summary, we have made a preliminary exploration of severely confined turbulent Rayleigh–Bénard convection over a wide range of width-to-height aspect ratio Γ, with $1/128 \leqslant \Gamma \leqslant 1$ and $3\times10^4 \leqslant Ra \leqslant 1\times10^{11}$. We first determined the Γ-dependence of the critical Ra for convection, $Ra_c = 482.4\Gamma^{-2.0\pm0.1}$, which is found to agree excellently with a previous theoretical result. The study then reveals how severe geometrical confinement induces transitions in global heat and momentum transport and in flow topology from the classical regime to a new regime characterized by steep scaling exponents and column-like plumes. For example, the scalings for $\Gamma = 1/128$ lying in the severely confined regime (Regime III) are $Nu-1\sim Ra^{0.61}$ and $Re\sim Ra^{0.80}$, which contrast sharply with $Nu-1\sim Ra^{0.31}$ and $Re\sim Ra^{0.52}$ observed at $\Gamma = 1$ in

Regime I. Based on the boundary separating the plume-controlled and severely confined regimes, a Rayleigh number for regime transition, $Ra^* = (29.37/\Gamma)^{3.23}$, has been identified. It is found that, for both Nu and Re, a rather sharp crossover in their scaling behaviours occurs at $Ra/Ra^* = 1.84 \times 10^{-5} Ra\Gamma^{3.23} = 1$. This relationship implies that the new scalings for Nu and Re can be observed over a wider range of Ra for smaller values of Γ.

Finally, we remark that the transition in severely confined RB convection is somewhat similar to that in rotating RB convection with the emergence of steep heat transfer scaling and columnar flow topology under extremely stabilizing conditions (severe confinement and vigorous rotation respectively). Though the analogy between confined RB and rotating RB convection needs to be made more quantitatively, the more well-studied rotating RB convection may provide insight into the steep scaling identified here and the formation of column-like plumes. As heat transport in severely confined environments exists widely in the modern electronics industry, our study should be of some relevance to certain engineering applications.

Acknowledgements

We thank S.-D. Huang for helpful discussions and M. Kaczorowski for his help with numerical simulations. This work was supported by the Hong Kong RGC (grant no. CUHK404513) and through a Hong Kong PhD Fellowship, and by a CUHK Direct Grant (project no. 3132740). We also thank the support of computational resources by the Leibnitz-Rechenzentrum Munich (project no. pr47vi).

References

AHLERS, G., GROSSMANN, S. & LOHSE, D. 2009 Heat transfer & large-scale dynamics in turbulent Rayleigh–Bénard convection. *Rev. Mod. Phys.* **81** (2), 503–537.

BAILON-CUBA, J., EMRAN, M. S. & SCHUMACHER, J. 2010 Aspect ratio dependence of heat transfer and large-scale flow in turbulent convection. *J. Fluid Mech.* **655**, 152–173.

BIZON, C., WERNE, J., PREDTECHENSKY, A. A., JULIEN, K., MCCORMICK, W. D., SWIFT, J. B. & SWINNEY, H. L. 1997 Plume dynamics in quasi-2D turbulent convection. *Chaos* **7** (1), 107–124.

BROWN, E., NIKOLAENKO, A. & AHLERS, G. 2005 Reorientation of the large-scale circulation in turbulent Rayleigh–Bénard convection. *Phys. Rev. Lett.* **95**, 084503.

CHENG, J. S., STELLMACH, S., RIBEIRO, A., GRANNAN, A., KING, E. M. & AURNOU, J. M. 2015 Laboratory-numerical models of rapidly rotating convection in planetary cores. *Geophys. J. Intl* **201** (1), 1–17.

CHILLÀ, F. & SCHUMACHER, J. 2012 New perspectives in turbulent Rayleigh–Bénard convection. *Eur. Phys. J.* E **35**, 1–25.

CHING, E. S. C. & TAM, W. S. 2006 Aspect-ratio dependence of heat transport by turbulent Rayleigh–Bénard convection. *J. Turbul.* **7**, 1–10.

CHONG, K. L., HUANG, S. D., KACZOROWSKI, M. & XIA, K. Q. 2015 Condensation of coherent structures in turbulent flows. *Phys. Rev. Lett.* **115**, 264503.

CIONI, S., CILIBERTO, S. & SOMMERIA, J. 1997 Strongly turbulent Rayleigh–Bénard convection in mercury: comparison with results at moderate Prandtl number. *J. Fluid Mech.* **335**, 111–140.

FUNFSCHILLING, D., BROWN, E., NIKOLAENKO, A. & AHLERS, G. 2005 Heat transport by turbulent Rayleigh–Bénard convection in cylindrical cells with aspect ratio one and larger. *J. Fluid Mech.* **536**, 145–154.

GROOMS, I., JULIEN, K., WEISS, J. B. & KNOBLOCH, E. 2010 Model of convective Taylor columns in rotating Rayleigh–Bénard convection. *Phys. Rev. Lett.* **104**, 224501.

GROSSMANN, S. & LOHSE, D. 2000 Scaling in thermal convection: a unifying theory. *J. Fluid Mech.* **407**, 27–56.

GROSSMANN, S. & LOHSE, D. 2001 Thermal convection for large Prandtl numbers. *Phys. Rev. Lett.* **86** (15), 3316.

GROSSMANN, S. & LOHSE, D. 2003 On geometry effects in Rayleigh–Bénard convection. *J. Fluid Mech.* **486**, 105–114.

HEWITT, D. R., NEUFELD, J. A. & LISTER, J. R. 2012 Ultimate regime of high Rayleigh number convection in a porous medium. *Phys. Rev. Lett.* **108**, 224503.

HUANG, S.-D., KACZOROWSKI, M., NI, R. & XIA, K.-Q. 2013 Confinement-induced heat-transport enhancement in turbulent thermal convection. *Phys. Rev. Lett.* **111**, 104501.

HUANG, S.-D. & XIA, K.-Q. 2016 Effects of geometric confinement in quasi-2-D turbulent Rayleigh–Bénard convection. *J. Fluid Mech.* **794**, 639–654.

KACZOROWSKI, M., CHONG, K.-L. & XIA, K.-Q. 2014 Turbulent flow in the bulk of Rayleigh–Bénard convection: aspect-ratio dependence of the small-scale properties. *J. Fluid Mech.* **747**, 73–102.

KACZOROWSKI, M., SHISHKIN, A., SHISHKINA, O. & WAGNER, C 2008 Development of a numerical procedure for direction simulations of turbulent convection in a closed rectangular cell. *New Results Numerical Exp. Fluids Mech. VI* **96**, 381–388.

KACZOROWSKI, M. & XIA, K.-Q. 2013 Turbulent flow in the bulk of Rayleigh–Bénard convection: small-scale properties in a cubic cell. *J. Fluid Mech.* **722**, 596–617.

KADANOFF, L. P. 2001 Turbulent heat flow: structures and scaling. *Phys. Today* **54** (8), 34–39.

KING, E. M., STELLMACH, S. & AURNOU, J. M. 2012 Heat transfer by rapidly rotating Rayleigh–Bénard convection. *J. Fluid Mech.* **691**, 568–582.

LOHSE, D. & XIA, K.-Q. 2010 Small-scale properties of turbulent Rayleigh–Bénard convection. *Annu. Rev. Fluid Mech.* **42**, 335–364.

NI, R., HUANG, S.-D. & XIA, K.-Q. 2015 Reversals of the large-scale circulation in quasi-2D Rayleigh–Bénard convection. *J. Fluid Mech.* **778**, R5.

NIKOLAENKO, A., BROWN, E., FUNFSCHILLING, D. & AHLERS, G. 2005 Heat transport by turbulent Rayleigh–Bénard convection in cylindrical cells with aspect ratio one and less. *J. Fluid Mech.* **523**, 251–260.

VAN DER POEL, E. P., STEVENS, R. J. A. M. & LOHSE, D. 2011 Connecting flow structures and heat flux in turbulent Rayleigh–Bénard convection. *Phys. Rev.* E **84** (4), 045303.

VAN DER POEL, E. P., STEVENS, R. J. A. M., SUGIYAMA, K. & LOHSE, D. 2012 Flow states in two-dimensional Rayleigh–Bénard convection as a function of aspect-ratio and Rayleigh number. *Phys. Fluids* **24**, 085104.

SHANG, X.-D., QIU, X.-L., TONG, P. & XIA, K.-Q. 2003 Measured local heat transport in turbulent Rayleigh–Bénard convection. *Phys. Rev. Lett.* **90**, 074501.

SHISHKINA, O., STEVENS, R. J. A. M, GROSSMANN, S. & LOHSE, D. 2010 Boundary layer structure in turbulent thermal convection and its consequences for the required numerical resolution. *New J. Phys.* **12**, 075022.

STEVENS, R. J. A. M., ZHONG, J. Q., CLERCX, H. J. H., AHLERS, G. & LOHSE, D. 2009 Transitions between turbulent states in rotating Rayleigh–Bénard convection. *Phys. Rev. Lett.* **103**, 024503.

SUN, C., REN, L.-Y., SONG, H. & XIA, K.-Q. 2005*a* Heat transport by turbulent Rayleigh–Bénard convection in cylindrical cells of widely varying aspect ratios. *J. Fluid Mech.* **542**, 165–174.

SUN, C., XI, H.-D. & XIA, K.-Q. 2005*b* Azimuthal symmetry, flowdynamics, and heat transport in turbulent thermal convection in a cylinder with an aspect ratio of 0.5. *Phys. Rev. Lett.* **95**, 074502.

WAGNER, S. & SHISHKINA, O. 2013 Aspect-ratio dependency of Rayleigh–Bénard convection in box-shaped containers. *Phys. Fluids* **25**, 085110.

WEI, P., WEISS, S. & AHLERS, G. 2015 Multiple transitions in rotating turbulent Rayleigh–Bénard convection. *Phys. Rev. Lett.* **114**, 114506.

WU, X.-Z. & LIBCHABER, A. 1992 Scaling relations in thermal turbulence: the aspect-ratio dependence. *Phys. Rev.* A **45** (2), 842–845.

XI, H.-D., LAM, S. & XIA, K.-Q. 2004 From laminar plumes to organized flows: the onset of large-scale circulation in turbulent thermal convection. *J. Fluid Mech.* **503** (47), 47–56.

XI, H.-D., ZHOU, Q. & XIA, K.-Q. 2006 Azimuthal motion of the mean wind in turbulent thermal convection. *Phys. Rev.* E **73** (5), 056312.

XIA, K.-Q. 2013 Current trends and future directions in turbulent thermal convection. *Theor. Appl. Mech. Lett.* **3**, 052001.

XIA, K.-Q. & LUI, S.-L. 1997 Turbulent thermal convection with an obstructed sidewall. *Phys. Rev. Lett.* **79**, 5006–5009.

YANG, Y., VERZICCO, R. & LOHSE, D. 2016 From convection rolls to finger convection in double-diffusive turbulence. *Proc. Natl Acad. Sci. USA* **113**, 69–73.

ZHOU, Q., LIU, B.-F., LI, C.-M. & ZHONG, B.-C. 2012 Aspect ratio dependence of heat transport by turbulent Rayleigh–Bénard convection in rectangular cells. *J. Fluid Mech.* **710**, 260–276.

ZHOU, Q. & XIA, K.-Q. 2010 Physical and geometrical properties of thermal plumes in turbulent Rayleigh–Bénard convection. *New J. Phys.* **12**, 075006.